JOURNAL OF SOLID STATE CHEMISTRY 119, 405–411 (1995)

Magnetic Properties of Tetravalent Praseodymium Perovskites $BaPrO_3$, $BaCe_yPr_{1-y}O_3$, and $Sr_yBa_{1-y}PrO_3$

Yukio Hinatsu[1]

Department of Chemistry, Japan Atomic Energy Research Institute, Tokai-mura, Ibaraki 319-11, Japan

Received March 13, 1995; in revised form June 12, 1995; accepted June 13, 1995

Tetravalent praseodymium perovskites $BaPrO_3$, $BaCe_yPr_{1-y}O_3$, and $Sr_yBa_{1-y}PrO_3$ were prepared, and their magnetic susceptibilities were measured in the temperature range between 4.2 and 300 K. Magnetic ordering found in the $BaPrO_3$ (the transition temperature is 11.6 K) is weakened with substitution of Sr for Ba and much more weakened with substitution of Ce for Pr. Above this transition temperature, the susceptibility decreases anomalously with increasing temperature. A magnetic hysteresis was found at 4.5 K for all the compounds studied here. The magnetic susceptibility above the transition temperature is composed of a Curie–Weiss term associated with a small effective magnetic moment of Pr^{4+} and a large temperature-independent paramagnetism. The effective magnetic moment of the Pr^{4+} ion in $Sr_yBa_{1-y}PrO_3$ increases with strontium concentration (y). This result is in accordance with the result obtained from the electron paramagnetic resonance spectrum of Pr^{4+} doped in $Sr_yBa_{1-y}CeO_3$. © 1995 Academic Press, Inc.

INTRODUCTION

The most stable oxidation state of rare earth elements is trivalent. In addition to this state, cerium, praseodymium, and terbium have the tetravalent state (1). We are interested in the electronic state of tetravalent praseodymium ions in solids.

Perovskite-type oxides, ABO_3, where A is a divalent ion (e.g. Sr, Ba), accommodate tetravalent metal ions at the B sites of the crystals. The B site ions sit at the center of the octahedron formed by six oxygen ions. Since tetravalent lanthanide and actinide ions can be incorporated into the B sites, this lattice type is useful for studying the magnetic properties of these ions in octahedral symmetry.

Our attention is given to the barium praseodymium oxide $BaPrO_3$. In our previous study (2), we have reported that this compound shows an antiferromagnetic transition at 11.5 K. A very sharp drop in the susceptibility is observed when the temperature is increased through this transition temperature. This magnetic ordering corresponds to the λ-type anomaly found in the heat capacity vs temperature curve (3). Above the transition temperature, the susceptibility follows the modified Curie–Weiss law. The effective magnetic moment of Pr^{4+} in $BaPrO_3$ is 0.68 μ_B. This result means that although the paramagnetic property of this compound is attributable to an unpaired $4f$ electron, the effect of the crystal field on the Pr^{4+} ion is great. This small effective magnetic moment can be explained by the octahedral crystal field model using the g value of the electron paramagnetic resonance (EPR) spectrum of Pr^{4+} doped in diamagnetic $BaCeO_3$ (which is isomorphous with $BaPrO_3$) (4).

To clarify the nature of magnetic interactions between praseodymium ions, we have prepared $BaCe_yPr_{1-y}O_3$ ($0 < y \leq 0.30$) solid solutions in which some diamagnetic Ce^{4+} ions are substituted for paramagnetic Pr^{4+} ions and $Sr_yBa_{1-y}PrO_3$ ($0 < y \leq 0.50$) solid solutions in which Sr^{2+} ions are substituted for Ba^{2+} ions, and measured both the temperature dependence of the magnetic susceptibilities between 4.2 K and room temperature and the field dependence of the magnetization at 4.5 and 20 K. To discuss the low effective magnetic moment of Pr^{4+} found in the $Sr_yBa_{1-y}PrO_3$ solid solutions and its variation with the y value, the EPR spectra of Pr^{4+} ions doped in $Sr_yBa_{1-y}CeO_3$ were measured.

EXPERIMENTAL

1. Sample Preparation

$BaPrO_3$. $BaCO_3$ and Pr_6O_{11} were used as the starting materials. Pr_6O_{11} was reduced to stoichiometric Pr_2O_3 by heating under a flow of hydrogen gas at 1000°C for 8 hr. $BaPrO_3$ was prepared by intimately grinding $BaCO_3$ and Pr_2O_3 in the correct stoichiometric metal ratio, pressing the mixture into a pellet, and then heating it under a flowing oxygen atmosphere at 1200°C in an SiC resistance furnace for a day. After cooling to room temperature, the sample was crushed into powder, reground, repressed into a pellet, and heated under the same conditions to make the reaction complete. Since $BaPrO_3$ loses a few oxygens at high tem-

[1] Present address: Department of Chemistry, Faculty of Science, Hokkaido University, Kita-ku, Sapporo 060, Japan.

0022-4596/95 $12.00

peratures and is reoxidized to the stoichiometric composition during cooling (5), the sample was kept at 1000°C for 48 hr and cooled to room temperature in the furnace.

$BaCe_yPr_{1-y}O_3$, $Sr_yBa_{1-y}PrO_3$. Starting materials are $BaCO_3$, Pr_6O_{11}, and CeO_2 for the preparation of $BaCe_yPr_{1-y}O_3$ solid solutions, and $BaCO_3$, $SrCO_3$, and Pr_6O_{11} for $Sr_yBa_{1-y}PrO_3$ solid solutions. Before use, CeO_2 was heated in air at 850°C to remove any moisture and oxidized to the stoichiometric composition. These materials were weighed in the correct metal ratios (y = 0.05, 0.10, 0.15, 0.20, 0.25, and 0.30 for $BaCe_yPr_{1-y}O_3$; y = 0.05, 0.10, 0.15, 0.20, 0.30, 0.40, and 0.50 for $Sr_yBa_{1-y}PrO_3$), mixed well, and then pressed into pellets. The heating procedures were the same as in the case of $BaPrO_3$ except for the heating temperature, which was raised to 1300°C to make the formation of solid solution complete.

$Sr_yBa_{1-y}Pr_{0.02}Ce_{0.98}O_3$. The samples for the measurements of EPR spectra of Pr^{4-} ions doped in diamagnetic $Sr_yBa_{1-y}CeO_3$ were prepared in the same manner as the preparation of $Sr_yBa_{1-y}PrO_3$ solid solutions. $BaCO_3$, $SrCO_3$, Pr_6O_{11}, and CeO_2 were weighed in the correct metal ratios (y = 0, 0.10, 0.30, and 0.50), mixed well, pressed into pellets, and then heated. After the mixtures were cooled, the grinding, mixing, and heating procedures were repeated to obtain homogeneous samples.

2. *Analysis*

An X-ray diffraction analysis was performed with Cu$K\alpha$ radiation on a Phillips PW 1390 diffractometer equipped with a curved graphite monochromator. The lattice parameters of the samples were determined by a least-squares method. The oxygen concentrations of the samples were checked by the weight change after heating. The results of the oxygen analysis indicate that in view of the error limits for this analysis, the samples prepared in this study are considered to have entirely ideal perovskite stoichiometry and therefore we use the formula ABO_3 to describe our samples.

3. *Magnetic Susceptibility Measurements*

The temperature dependence of the magnetic susceptibilities was measured both with a Faraday-type torsion balance and with a commercial SQUID magnetometer (Quantum Design, MPMS model).

The temperature range of the magnetic susceptibility measurements with the magnetic balance was between 4.2 K and room temperature. The apparatus was calibrated with $CoHg(SCN)_4$ as a standard (6). The temperature of the sample was measured by a "normal" Ag vs Au–0.07 at.% Fe thermocouple (4.2 ~ 40 K) (7) and an Au–Co vs Cu thermocouple (10 K ~ room temperature). The magnetization was measured in each of the field strengths 2800, 4700, 6900, 9000, and 10,600 G. Details of the experimental procedure have been described elsewhere (8).

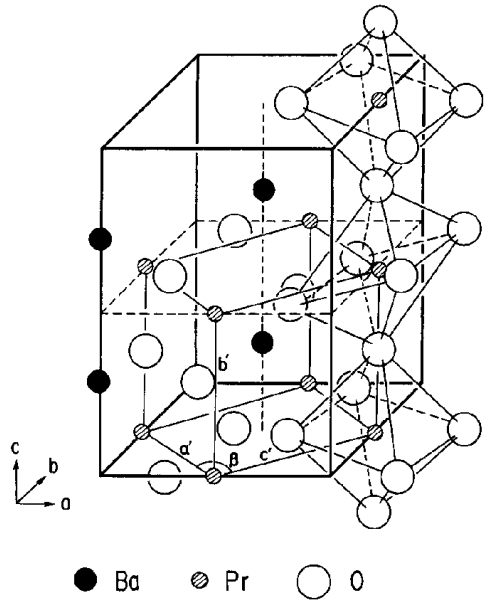

FIG. 1. Crystal structure of $BaPrO_3$.

The magnetic susceptibility measurements with the SQUID magnetometer were carried out at 1000 G in the temperature range between 4.5 and 300 K. The field dependence of the magnetization for the samples was measured at 4.5 and 20 K by changing the magnetic field strength from 0 to 50,000 G, from 50,000 to 0 G, from 0 to −50,000 G, from −50,000 to 0 G, and then from 0 to 50,000 G.

4. *Electron Paramagnetic Resonance Measurements*

The EPR measurements were carried out with a JEOL RE-2X spectrometer operating at X-band frequency (9.1 GHz) with 100-kHz field modulation. Measurements were made both at room temperature and at 4.2 K. The magnetic field was swept from 100 to 13,000 G. Before the specimen was measured, a blank was recorded to eliminate the possibility of interference by the background resonance of the cavity and/or sample tube. The magnetic field was monitored with a proton NMR gaussmeter, and the microwave frequency was measured with a frequency counter.

RESULTS AND DISCUSSION

$BaPrO_3$

The $BaPrO_3$ crystallizes orthorhombically. Figure 1 shows its crystal structure. The lattice parameters for the $BaPrO_3$ prepared in this study are a = 6.188, b = 6.205, and c = 8.738 Å. As shown in Fig. 1, in the true crystallographic cell, there are four distorted perovskite pseudocells. They are monoclinic and their cell parameters are

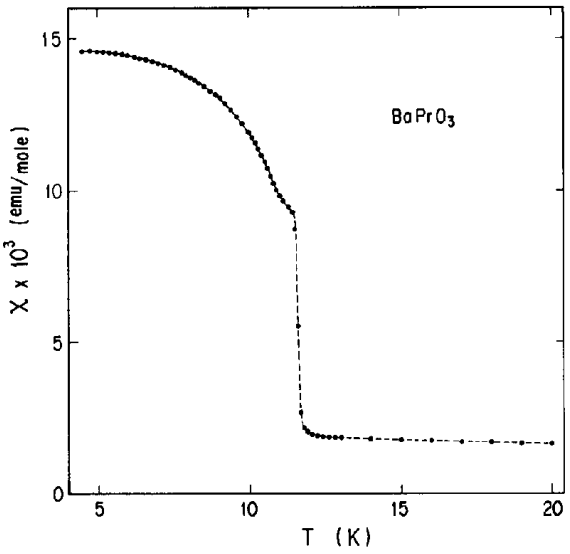

FIG. 2. Temperature dependence of magnetic susceptibility for Ba PrO_3 measured by SQUID.

calculated to be $a' = c' = 4.382$, $b' = 4.369$ Å, and $\beta = 90.16°$. This result ($a' \simeq b' \simeq c'$ and $\beta \simeq 90°$) means that the orthorhombic distortion from cubic perovskite is quite small and the Pr^{4+} ion is nearly octahedrally coordinated by six oxygen ions, although there is a cooperative buckling of octahedra (see Fig. 1). Figure 2 shows the temperature dependence of the magnetic susceptibility for $BaPrO_3$ measured in a magnetic field of 1000 G by the SQUID. A very sharp decline in the susceptibility is observed when the temperature is increased through the transition temperature (11.6 K). This result is in accordance with the magnetic susceptibility data previously measured by the magnetic torsion balance (2).

Figure 3 shows the magnetic hysteresis curve (magnetization vs applied field curve) for $BaPrO_3$ at 4.5 K measured by the SQUID. A weak hysteresis has been found, i.e., the magnetic susceptibility of $BaPrO_3$ depends on the applied field at this temperature. The small ferromagnetic moment

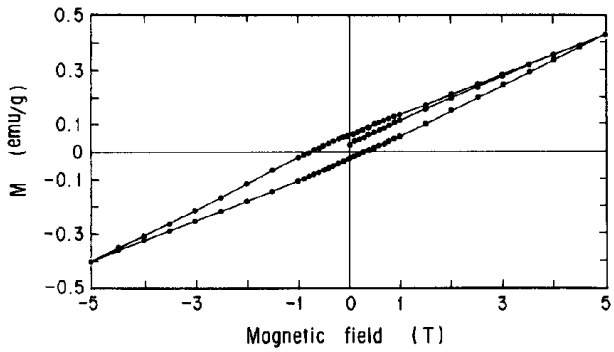

FIG. 3. Magnetic hysteresis curve for $BaPrO_3$ at 4.5 K.

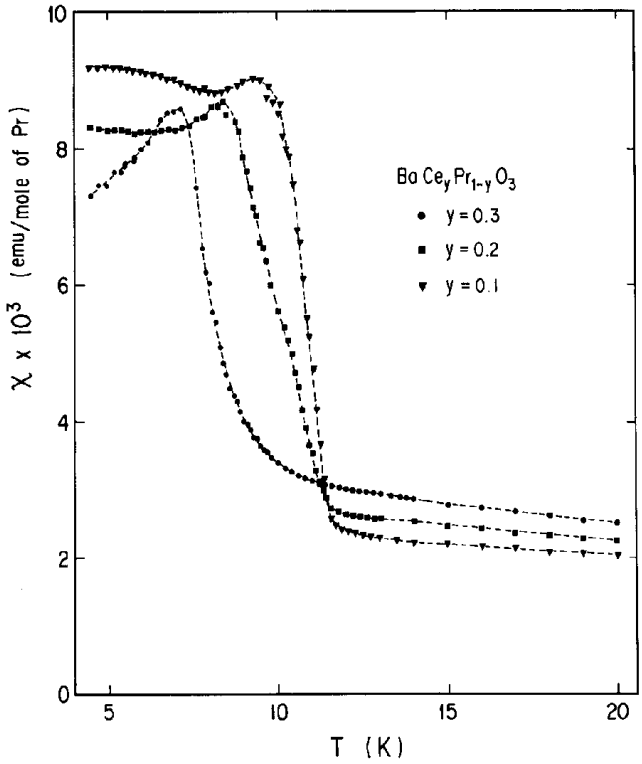

FIG. 4. Magnetic susceptibilities for $BaCe_yPr_{1-y}O_3$ solid solutions (y = 0.10, 0.20, and 0.30) at low temperatures measured by SQUID.

may derive from a minor departure from chemical stoichiometry. At 20 K, which is higher than the magnetic transition temperature, no hysteresis has been found and the behavior of $BaPrO_3$ is paramagnetic.

$BaCe_yPr_{1-y}O_3$

From the X-ray powder diffraction analysis, the orthorhombic solid solutions of $BaPrO_3$ and $BaCeO_3$ were found to be formed in a single phase. Figure 4 shows the temperature dependence of the magnetic susceptibilities for $BaCe_yPr_{1-y}O_3$ (y = 0.10, 0.20, and 0.30) in a magnetic field of 1000 G measured by the SQUID. As expected, magnetic interactions between praseodymium ions are weakened with the substitution of cerium for praseodymium. Figure 5 shows the variation of the transition temperatures for $BaCe_yPr_{1-y}O_3$ with cerium concentration, y. The transition temperature decreases greatly with the substitution of cerium for praseodymium, because this substitution decreases the concentration of praseodymium ions, i.e., the magnetic dilution increases with y.

Below the transition temperatures, the magnetic susceptibilities of these solid solutions also depend on the applied magnetic field. Figure 6 shows the magnetic hysteresis curve for $BaCe_{0.25}Pr_{0.75}O_3$ at 4.5 K, which is very similar to that for $BaPrO_3$.

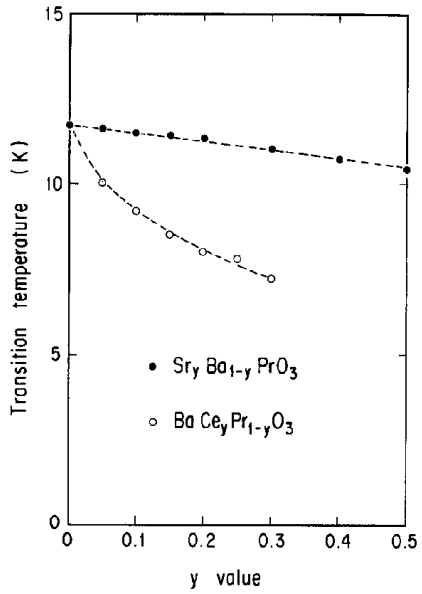

FIG. 5. Variation of magnetic transition temperature with y value for $BaCe_yPr_{1-y}O_3$ solid solutions and $Sr_yBa_{1-y}PrO_3$ solid solutions.

$Sr_yBa_{1-y}PrO_3$

The X-ray powder diffraction analysis shows that the orthorhombic solid solutions of $BaPrO_3$ and $SrPrO_3$ were formed in a single phase at least in the experimental Sr/(Ba + Sr) ratios ($y = 0 \sim 0.50$).

Figure 7 shows the variation of the lattice parameters, a, b, and c, for $Sr_yBa_{1-y}PrO_3$ solid solutions as a function of strontium concentration (y). With increasing strontium concentration, all the lattice parameters decrease, due to the substitution of smaller Sr^{2+} ions for Ba^{2+} ions. Since the difference in ionic radius between Sr^{2+} and Ba^{2+} is not very large (9), this substitution of Sr^{2+} for Ba^{2+} in $Sr_yBa_{1-y}PrO_3$ results in only minor shrinkage of the lattice. For example, the decrease in the lattice parameter of $Sr_{0.50}Ba_{0.50}PrO_3$ is only $\simeq$1% compared with that of Ba PrO_3. As shown already, the orthorhombic distortion from ideal cubic perovskite structure is quite small for $BaPrO_3$. This situation is valid for the $Sr_yBa_{1-y}PrO_3$ solid solutions studied here. These facts indicate that the change in the crystal field is negligible among these $Sr_yBa_{1-y}PrO_3$ solid solutions and the Pr^{4+} ion is nearly octahedrally coordinated by six oxygen ions.

Figure 8 shows the temperature dependence of the magnetic susceptibilities for $Sr_yBa_{1-y}PrO_3$. This figure indicates that the temperature dependence of the susceptibilities is quite similar to that found for $BaPrO_3$. A very sharp decline in the susceptibility is still observed when the temperature is increased through the transition temperature even for the $Sr_{0.50}Ba_{0.50}PrO_3$ solid solution. The variation of the transition temperature for $Sr_yBa_{1-y}PrO_3$ solid solutions with strontium concentration (y) is shown in Fig. 5. The

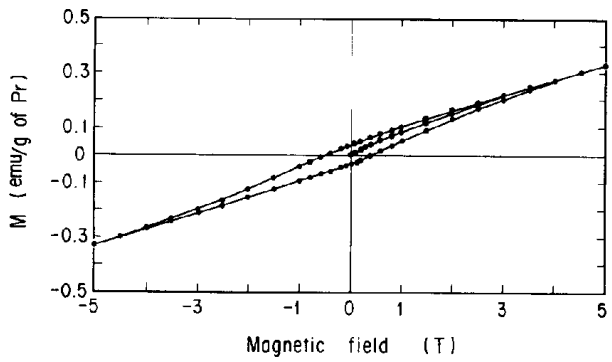

FIG. 6. Magnetic hysteresis curve for $BaCe_{0.25}Pr_{0.75}O_3$ at 4.5 K.

transition temperatures of $Sr_yBa_{1-y}PrO_3$ solid solutions decrease with increasing y value, but the rate of this decrease is much slower than that found for $BaCe_yPr_{1-y}O_3$ solid solutions. This is due to the fact that the substitution of Sr for Ba in $BaPrO_3$ does not decrease the Pr^{4+} concentration in the lattice; $SrPrO_3$ is paramagnetic.

The hysteresis of the magnetization has been also found in these $Sr_yBa_{1-y}PrO_3$ solid solutions. Figure 9 shows the magnetic hysteresis curve (magnetization vs applied magnetic field curve) for $Sr_{0.20}Ba_{0.80}PrO_3$ at 4.5 K. From the comparison with Fig. 3, this figure indicates that the field dependence of the magnetization for $Sr_yBa_{1-y}PrO_3$ is somewhat different from that for $BaPrO_3$ at low applied field.

Effective Magnetic Moment of Pr^{4+} in $Sr_yBa_{1-y}PrO_3$

Above the transition temperatures, the magnetic susceptibilities of these $Sr_yBa_{1-y}PrO_3$ solid solutions follow the

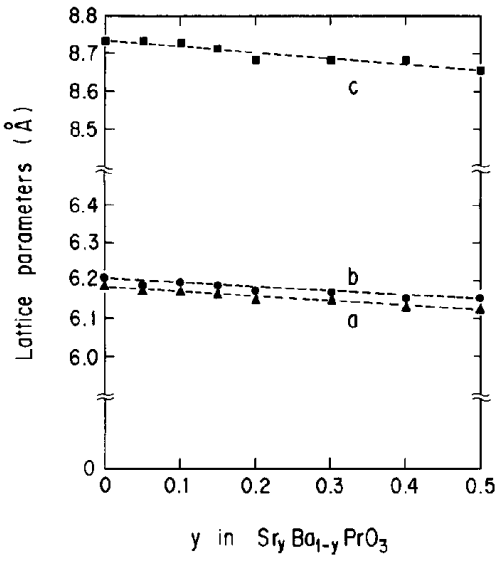

FIG. 7. Variation of lattice parameters for $Sr_yBa_{1-y}PrO_3$ solid solutions with y value.

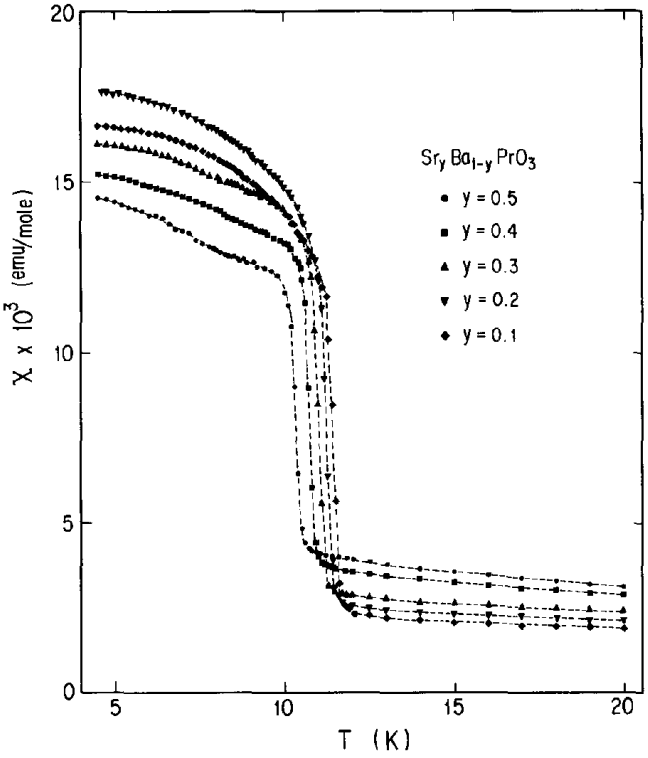

FIG. 8. Magnetic susceptibilities for $Sr_yBa_{1-y}PrO_3$ solid solutions (y = 0.10, 0.20, 0.30, 0.40, and 0.50) at low temperatures measured by SQUID.

modified Curie–Weiss law. From the extrapolation of the measured magnetic susceptibility (χ_{exp}) to $1/T \rightarrow 0$, the temperature-independent paramagnetism (χ_{TIP}) was obtained. The resulting temperature-dependent susceptibility ($\chi(T) = \chi_{exp} - \chi_{TIP}$) followed the Curie–Weiss law. The effective magnetic moments of praseodymium can be calculated from this temperature-dependent part of the susceptibility; they are listed in Table 1. The effective magnetic moments obtained are much smaller than that expected for a free f^1 ion (2.54 μ_B), which indicates that the crystal

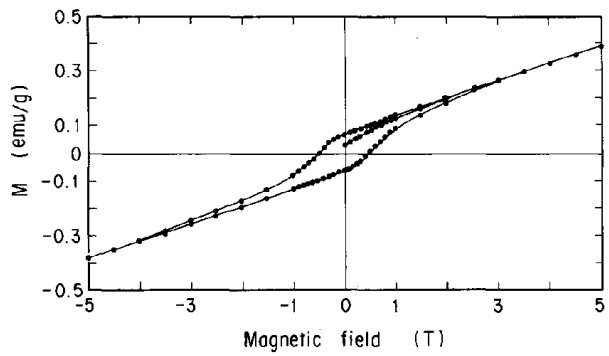

FIG. 9. Magnetic hysteresis curve for $Sr_{0.20}Ba_{0.80}PrO_3$ at 4.5 K.

TABLE 1
Magnetic Data for $Sr_yBa_{1-y}PrO_3$

Solid solutions	μ_{eff} (μ_B)	χ_{TIP} (emu/mole)
$Sr_{0.1}Ba_{0.9}PrO_3$	0.812	620×10^{-6}
$Sr_{0.2}Ba_{0.8}PrO_3$	0.834	630×10^{-6}
$Sr_{0.3}Ba_{0.7}PrO_3$	0.833	650×10^{-6}
$Sr_{0.4}Ba_{0.6}PrO_3$	0.835	650×10^{-6}
$Sr_{0.5}Ba_{0.5}PrO_3$	0.879	730×10^{-6}

field with octahedral symmetry has a significant effect on the magnetic properties of Pr^{4+}. A comparable small magnetic moment has been reported for the actinide ion with $[Rn]5f^1$ configuration ([Rn]: Rn core) in the same octahedral crystal field (10, 11).

The effective magnetic moment of Pr^{4+} in the $Sr_yBa_{1-y}PrO_3$ increases with strontium concentration (y). The substitution of Sr for Ba in $Sr_yBa_{1-y}PrO_3$ changes neither the Pr^{4+} concentration in the solid solutions nor the crystal field around the Pr^{4-} ion. This increase in the effective moment of Pr^{4+} is due to the fact that the effective magnetic moment for $SrPrO_3$ (μ_{eff} = 1.58 μ_B) (12) is larger than that for $BaPrO_3$ (μ_{eff} = 0.68 μ_B) (2), and is in accordance with the behavior found in the g value of the EPR spectrum for the Pr^{4+} ion doped in $Sr_yBa_{1-y}CeO_3$ (which is isomorphous with $Sr_yBa_{1-y}PrO_3$), as will be described later.

The values of the temperature-independent paramagnetism (χ_{TIP}) obtained are in the range between 6.2×10^{-4} and 7.3×10^{-4} emu/mole, i.e., they are nearly constant for the $Sr_yBa_{1-y}PrO_3$ solid solutions. We have already shown that the large temperature-independent paramagnetism ($\chi_{TIP} = 6.8 \times 10^{-4}$ emu/mole) found for $BaPrO_3$ can be explained by the magnetic susceptibility calculation based

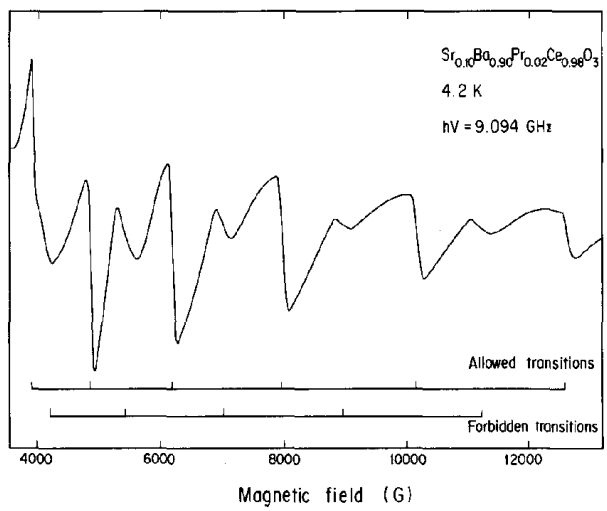

FIG. 10. EPR spectrum of Pr^{4+} ion doped in $Sr_{0.10}Ba_{0.90}CeO_3$ at 4.2 K.

TABLE 2
Experimental and Calculated Line Positions[a] for $Sr_{0.1}Ba_{0.9}PrO_3$

Experimental		Calculated		Difference
Allowed	Forbidden	Allowed	Forbidden	exp − calc
12,814		12,793		21
	11,366		11,374	−8
10,204		10,205		−1
	8,989		8,986	3
7,971		7,984		−13
	7,004		6,999	5
6,184		6,199		−15
	5,450		5,452	−2
4,853		4,850		3
			4,307	—
3,903		3,869		34

[a] All values are given in G.

on the octahedral crystal field model (4). Since the change in the crystal field around the Pr^{4+} ion by substitution of Sr for Ba in $Sr_yBa_{1-y}PrO_3$ is negligible, the temperature-independent paramagnetism will not change in these solid solutions; i.e., a small energy gap between the ground and excited crystal field energy levels (~2000 cm^{-1}) (13) produces large temperature-independent paramagnetism ($\chi_{TIP} \sim 6 \times 10^{-4}$ emu/mole) (4).

Electron Paramagnetic Resonance of Pr^{4+} Doped in $Sr_yBa_{1-y}CeO_3$

For the praseodymium ion in the tetravalent state, an EPR spectrum should be observed because the Pr^{4+} ion is a Kramers ion ([Xe]$4f^1$ configuration). Our previous study (4) shows that the EPR spectra of Pr^{4+} can be observed by diluting it in a diamagnetic $BaCeO_3$ (which is isomorphous with $BaPrO_3$ (14)). So, in this study, we have prepared the samples for the EPR measurements in which Pr^{4+} ion is doped in the $Sr_yBa_{1-y}CeO_3$.

At room temperature, no EPR spectra were measured. At 4.2 K, the EPR spectra could be measured. The observation of the EPR spectra means that the praseodymium ion is not in the trivalent state, but in the tetravalent state (15). With increasing strontium concentration, the spectra became broader.

For the EPR spectrum of Pr^{4+} doped in $BaCeO_3$, a very large hyperfine interaction with the ^{141}Pr nucleus (nuclear spin $I = 5/2$) was observed. In addition to the allowed hyperfine transitions, forbidden hyperfine transitions were observed. The number of observed transitions is, therefore, 11. The experimental results and analysis for the EPR spectrum of this Pr^{4+} ion in $BaCeO_3$ have been reported previously (4).

Figure 10 shows the EPR spectrum for Pr^{4+} ion doped in $Sr_{0.1}Ba_{0.9}CeO_3$. Forbidden hyperfine transitions have still been found. For the case of Pr^{4+} ion in $Sr_yBa_{1-y}CeO_3$ with $y \geq 0.3$, forbidden transitions are no longer found. This is probably due to the broadness of the EPR spectra.

The isotope ^{141}Pr (natural abundance: 100%) has a nuclear spin of $I = 5/2$ and a nuclear magnetic moment of +4.3 nuclear magnetons. The spin Hamiltonian for the EPR spectrum of Pr^{4+} in $Sr_yBa_{1-y}CeO_3$ is

$$H = g\beta\mathbf{H}\cdot\mathbf{S}' + A\mathbf{I}\cdot\mathbf{S}' - g'_N\beta\mathbf{H}\cdot\mathbf{I}, \qquad [1]$$

where g is the g value for the Pr^{4+} ion with an effective spin $S' = 1/2$, A is the hyperfine coupling constant, g'_N is the effective nuclear g value (in units of μ_B), β is the Bohr magneton, and $\mathbf{H}$ is the applied magnetic field. Usually the electronic Zeeman term is much larger than the hyperfine term, which would result in a six-line spectrum for an isotropic resonance with $I = 5/2$. In this case, the hyperfine interaction with the ^{141}Pr nucleus is so large that the above Hamiltonian must be solved exactly. The solution is well known (Breit–Rabi equation) and has been given by Ramsey (16) and others (17).

The resulting of fitting the observed EPR spectra of $Pr^{4+}/Sr_{0.1}Ba_{0.9}CeO_3$ to the parameters of the spin Hamiltonian are shown in Table 2, with the best-fit parameters $|g| = 0.740$, $A = 0.0610$ cm^{-1} with g_N set equal to 0.0. The sign of the g value should be negative, from the comparison with other f^1 systems in octahedral symmetry, such as NpF_6/UF_6 (18) and Pa^{4+}/Cs_2ZrCl_6 (17), where the sign of the g value has been measured. The parameters of $|g|$ and A for the Pr^{4+} ions in $Sr_yBa_{1-y}CeO_3$ ($y = 0$, 0.1, 0.3, and 0.5) are given in Table 3. The hyperfine coupling constants A are constant irrespective of the y value. On the other hand, the $|g|$ value increases with the y value. This trend for the g value against the y value is in accordance with the increase of the effective magnetic moment of Pr^{4+} ion in $Sr_yBa_{1-y}PrO_3$ with the y value.

The effective magnetic moment is calculated from the g value by the relation $\mu_{eff} = g\sqrt{S(S+1)}$ (S is the spin quantum number). For example, the g value for the Pr^{4+}

TABLE 3
Hyperfine Coupling Constant and g Value for Pr^{4+} in $Sr_yBa_{1-y}CeO_3$

Host solid solutions	A (cm^{-1})	$\|g\|$
$BaCeO_3$	0.0609	0.741
$Sr_{0.1}Ba_{0.9}CeO_3$	0.0610	0.740
$Sr_{0.3}Ba_{0.7}CeO_3$	0.0608	0.746
$Sr_{0.5}Ba_{0.5}CeO_3$	0.0609	0.752

in $BaCeO_3$ obtained from the analysis of its EPR spectrum is 0.741. Then the effective magnetic moment of Pr^{4+} is calculated to be 0.642 μ_B, which is close to the moment of $BaPrO_3$ (0.68 μ_B) derived from the magnetic susceptibility measurement. Since the effect of crystal field on the Pr^{4+} ion in the $SryBa_{1-y}CeO_3$ solid solutions changes very little with Sr substitution for Ba (y value), the increase in the g value with y is slight. On the other hand, the increase in the effective magnetic moment of $Sr_yBa_{1-y}PrO_3$ with y is great due to the large difference in the effective magnetic moment between $BaPrO_3$ (0.68 μ_B) and $SrPrO_3$ (1.58 μ_B). Therefore, some discrepancy has been found between the moment calculated from the relation $\mu_{eff} = g\sqrt{S(S+1)}$ and the moment obtained from the magnetic susceptibility measurement for $Sr_yBa_{1-y}PrO_3$ solid solutions with large y values.

REFERENCES

1. N. E. Topp, "Chemistry of the Rare-Earth Elements." Elsevier, Amsterdam, 1965.
2. Y. Hinatsu, *J. Solid State Chem.* **102,** 362 (1993).
3. J. B. Bulman, M. V. Kuric, R. P. Guertin, S. Foner, E. J. McNiff, Jr., G. Cao, J. O'Riely, J. E. Crow, P. P. Wise, and T. Yuen, *J. Appl. Phys.* **69,** 4874 (1991).
4. Y. Hinatsu and N. Edelstein, *J. Solid State Chem.* **112,** 53 (1994).
5. M. Yoshimura, T. Nakamura, and T. Sata, *Bull. Tokyo Inst. Technol.* **120,** 13 (1974).
6. H. St. Rade, *J. Phys. Chem.* **77,** 424 (1973).
7. L. L. Sparks and R. L. Powell, *J. Res. Nat. Bur. Stand. (U.S.) A* **76,** 263 (1972).
8. Y. Hinatsu and T. Fujino, *J. Solid State Chem.* **60,** 195 (1985).
9. R. D. Shannon, *Acta Crystallogr. Sect. A* **32,** 751 (1976).
10. B. Kanellakopulos, "Gmelin Hanbduch der Annorgannischen Chemie," Uranium Supplement Vol. A6, p. 19. Springer-Verlag, Berlin, 1983.
11. M. Bickel and B. Kanellakopulos, *J. Solid State Chem.* **107,** 273 (1993).
12. Y. Hinatsu, unpublished results.
13. S. Kern, C.-K. Loong, and G. H. Lander, *Phys. Rev. B* **32,** 3051 (1985).
14. A. J. Jacobson, B. C. Tofield, and B. E. F. Fender, *Acta Crystallogr. Sect. B* **28,** 956 (1972).
15. A. Abragam and B. Bleaney, "Electron Paramagnetic Resonance of Transition Ions." Oxford Univ. Press, London, 1970.
16. N. F. Ramsey, "Molecular Beams." Clarendon, Oxford, 1956.
17. J. D. Axe, H. J. Stapleton, and C. D. Jeffries, *Phys. Rev.* **121,** 1630 (1961).
18. C. A. Hutchison and B. Weinstock, *J. Phys. Chem.* **32,** 56 (1960).